catalysts

MDPI

Article

Au Capping Agent Removal Using Plasma at Mild Temperature

Indra Puspitasari [1], Emmanuel Skupien [1], Freek Kapteijn [1] and Patricia J. Kooyman [1,2,*]

[1] Catalysis Engineering, ChemE, Delft University of Technology, Van der Maasweg 9, 2629 HZ Delft, The Netherlands; i.puspitasari@tudelft.nl (I.P.); e.skupien@tudelft.nl (E.S.); f.kapteijn@tudelft.nl (F.K.)

[2] ChemEng, University of Cape Town, Private Bag X3, 7701 Rondebosch, South Africa

* Correspondence: patricia.kooyman@uct.ac.za; Tel.: +27-21-650-2732

Academic Editors: Leonarda F. Liotta and Salvatore Scirè

Received: 15 September 2016; Accepted: 1 November 2016; Published: 17 November 2016

Abstract: To prevent sintering, ozone treatment at mild temperature is used to remove the capping agent from supported Au nanoparticles. The Au nanoparticles are first synthesized as a colloidal solution and then supported on alumina. Fourier Transform Infra Red (FTIR) shows the capping agent is removed completely. Transmission Electron Microscopy (TEM) and catalytic test reactions show the Au does not sinter significantly upon low temperature ozone treatment.

Keywords: Au nanoparticle synthesis; characterization; immobilization; capping agent removal; ozonication; benzyl alcohol oxidation; CO oxidation

1. Introduction

Metallic nanoparticles have many applications including being used as catalysts, chemical and biological sensors, and quantum dots; they are also used for drug delivery [1–4]. Their controlled synthesis, which yields narrow particle size distributions, is still open for improvement.

Capping agents are commonly used in the preparation of metal nanoparticles [5–11]. The function of the capping agent is to avoid aggregation of the nanoparticles in the solution and to control both the size and shape of the nanoparticles [8–11]. This can lead to monodisperse metal nanoparticles with a pre-determined size. However, after nanoparticle preparation, the capping agent is still attached to the surface of the nanoparticles and may hamper the accessibility of the catalytic surface for reactants. When the metal nanoparticles are used in catalytic reactions, the presence of the capping agent decreases the catalytic activity and selectivity because it hinders the chemical and physical access to the metal particle surface and modifies the surface chemistry of the metal surface [12]. The capping agent needs to be removed prior to most applications, but as the capping agent stabilises the nanoparticles, its removal might induce undesired changes in nanoparticle size and/or shape and change the interaction with the support (in the case of supported particles).

The most straightforward method for removing the capping agent is calcination [13–15], but the high temperature involved (often around 400 or 500 °C) induces mobility of the metal atoms and, thus, changes in particle shape and size (notably sintering to larger particle size and broadening of the particle size distribution). Lange et al. [13] showed that calcination of Poly(vinyl-pyrrolidone) (PVP)-capped Pt nanoparticles leads to the removal of the protective PVP shell surrounding the colloids, resulting in an increase in both surface area and Pt particle size. The resulting catalysts showed lower selectivity for 2-hexyne hydrogenation. Imura et al. [14] state that "almost all of the capping agent" is removed from their Au nanoflowers by washing, whereas calcination, even at the very low temperature of 100 °C, already changes the morphology of the nanoflowers. Calcination at 400 °C or above leads to completely spherical nanoparticles that have lost all their specific nanoflower

structure. The washing procedure leads to the best catalytic properties, even though some capping agent is still present. The starting material with all capping agent present is the worst catalyst, clearly showing that the capping agent needs to be removed before the catalytic reaction. Zhong et al. [15] used lysine as the capping agent and also report much improved catalytic performance after removal of the capping agent. Unfortunately, they do not include detailed particle size analysis so the effect of their calcination method at 300 °C remains unresolved. Chen et al. [16] use an electrochemical method to remove the capping agent, which also involved adding PbO_2. Although the catalytic performance of these Au nanoparticles after the cleaning treatment has improved a lot, it is not quite clear what the role of the Pb is. Recourse has been sought in washing with chemicals (solvent for the capping agent, or acid, base, or salt solution) [17–20] and the combination of Ultraviolet and ozone (UVO) treatments [20]. The disadvantage of all these methods is that, often, either the nanoparticle size or shape changes. The disadvantage of UVO treatment is that two sources of energy are required in a small reaction volume, and the temperature of the reaction cannot be tuned easily as the UV source inevitably also releases heat into the system.

It would be highly beneficial to remove the capping agent in the gas phase at (close to) room temperature, as this would prevent the mobility of the metal atoms and thus the detrimental effect on particle size and shape. In an effort to reduce the temperature required, ozone treatment has been used to remove unwanted organic compounds from inorganic surfaces [21,22]. In this method, a sample is contacted with an oxygen/ozone mixture at a certain temperature where ozone decomposes into atomic oxygen and radical species, which are highly reactive [23,24]. Kuhn et al. used ozone treatment at 200 °C to remove the template from all-silica decadodecasil 3R (DD3R) zeolites in a 38 h detemplation process [21]. As a comparison to the ozone-treated samples, the synthesized samples were also calcined at 550–700 °C for 6–16 h. The porosity characteristics of the ozone-treated samples were equal to those of the calcined samples, which verifies that the ozone treatment at low temperature is a powerful detemplation method. Menard et al. [25] showed decreased sintering after ozone treatment as compared to classical calcination for titania-supported Au nanoparticles, but they did not investigate whether any residue of their S-containing capping agent was still present. Recently, another study on ozone treatment for capping agent removal from Au nanoparticles was published [26]. This study tackled a stronger binding S-containing capping agent, which was partially oxidised by mild ozone treatment and then washed off using water. Depending on the duration of the ozone treatment, only a part of the capping agent was removed. We have chosen to use an N-containing capping agent as that intrinsically binds less strongly to metal nanoparticles than S-containing capping agents do.

In the 1980s, Haruta showed that oxide-supported gold nanoparticles with particle size smaller than 5 nm have remarkable catalytic activity even at low temperatures (see [1] for a review). Ever since, gold nanoparticles have been recognized for many reactions, including oxidation of propene [27,28], CO oxidation [29], NO_x reduction [30,31], selective hydrogenation of acetylene [32,33], and the water-gas shift reaction [34,35]. Gold nanoparticles have been successfully prepared using several capping agents. Fatty amines are among the most successfully used capping agents [36,37], and dodecylamine (DDA) was used for the current study. No literature reports have been found using ozone to obtain pure gold nanoparticles starting from DDA-mediated synthesis.

We report DDA capping agent removal from the surface of supported Au nanoparticles using ozone treatment. The experiments were conducted at mild conditions to prevent structural and morphological changes as well as agglomeration of the nanoparticles. The catalyst characterization was performed using Transmission Electron Microscopy (TEM), Fourier Transform Infrared Spectroscopy (FTIR), and X-ray Photoelectron Spectroscopy (XPS). CO oxidation and selective oxidation of benzyl alcohol to benzaldehyde were performed to study the catalytic performance before and after capping agent removal.

2. Results and Discussion

2.1. Catalyst Characterization

The use of capping agent yields a uniform particle size as shown in Figure 1. The Au-DDA colloid showed severe carbon contamination in the TEM, because the excess of DDA was still present in the colloid and was being cracked by the electron beam (Figure 1a). The average particle size of the Au-DDA colloid is 3.3 nm (St.Dev. = 0.5). Figure 1b shows a TEM image of the Au-DDA colloid (w). The average particle size is 3.8 nm (St.Dev. = 0.5). The inset in Figure 1b shows that the Au nanoparticles are monocrystalline as reported by Quintanilla et al [12]. As expected, the immobilisation of the Au nanoparticles on the γ-Al_2O_3 support does not drastically change the particle size (Figure 2a) because the gold particles had been produced before the deposition, and the deposition process should not alter the particle size and distribution [38]. The average particle size of as-prepared particles and that of particles after complete capping agent removal using ozone treatment at 30 °C was 4.0 nm (St.Dev. = 0.8) and 4.3 nm (St.Dev. = 1.0), respectively (Figure 2a,b). The broadening of the particle size distribution after ozone treatment shows that some sintering happened. Ozone treatment leads to slight sintering and slight broadening of the particle size distribution. However, since the ozone treatment is at a mild temperature, the sintering is less than that at high temperatures. For a sulphur-containing capping agent, Menard et al. showed a tripling of the nanoparticle size (from 0.8 to 2.7 nm) upon calcination at 400 °C, whereas the particle size increase was limited to 1.2 nm after ozone treatment [25]. Elliott et al. [26] found that slight sintering only occurred after all capping agent had been removed by the ozone treatment. The particle size stayed at 1.4 nm upon partial capping agent removal and increased to 1.6 nm when the S signal was no longer observed in the XP spectra. Figure 2b (inset) shows that the ozone treatment does not change the Au nanoparticle crystallinity.

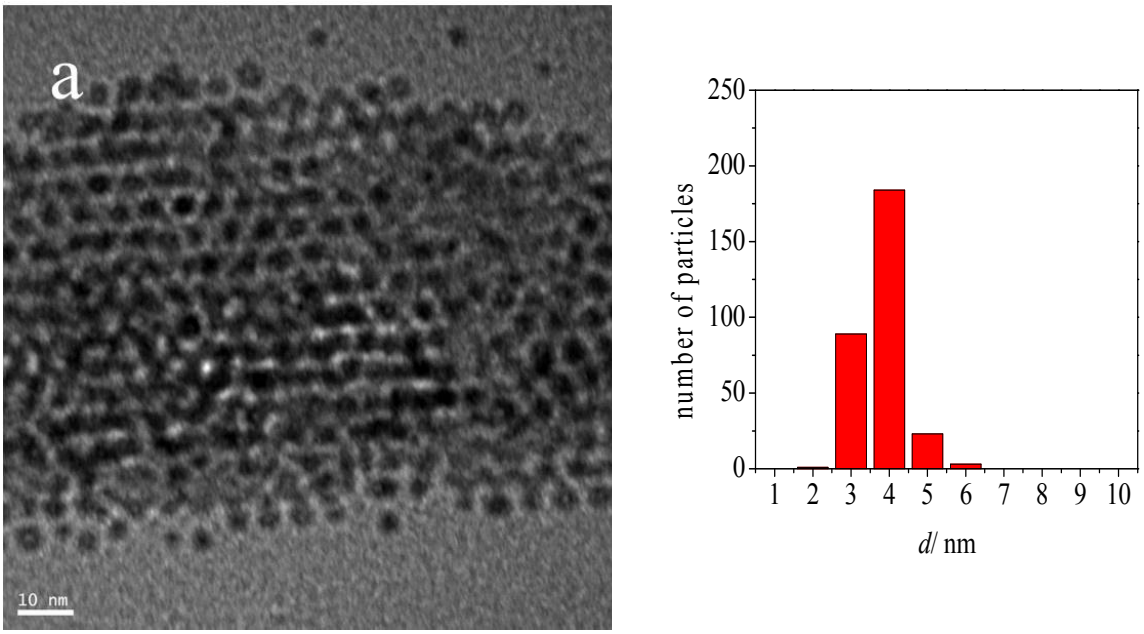

Figure 1. *Cont.*

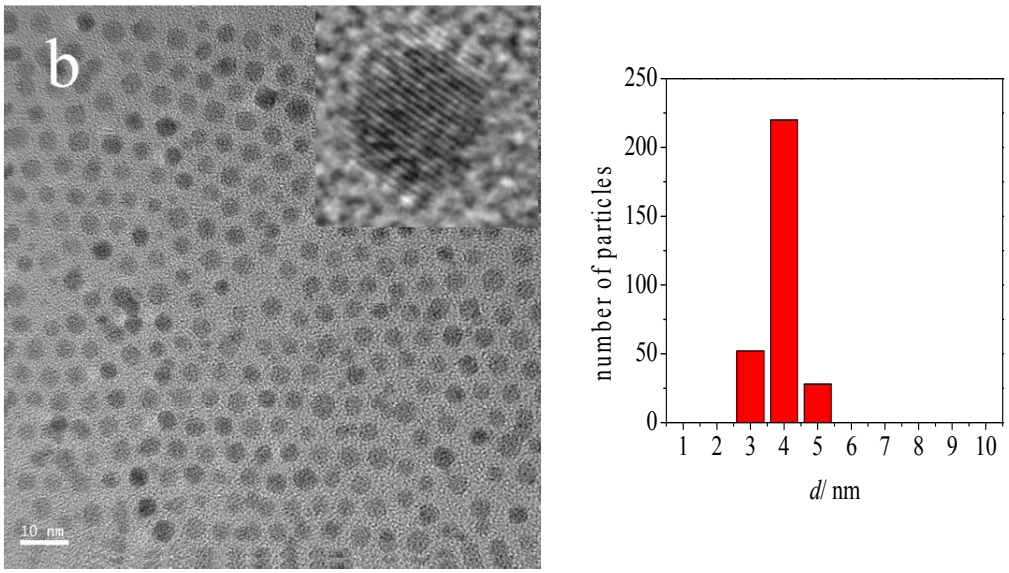

Figure 1. Transmission Electron Microscopy (TEM) images (left) and particle size distributions (right) of (**a**) Au-dodecylamine (DDA) colloid; and (**b**) Au-DDA colloid (w). The inset in the TEM image (**b**) shows the crystallinity of an Au nanoparticle.

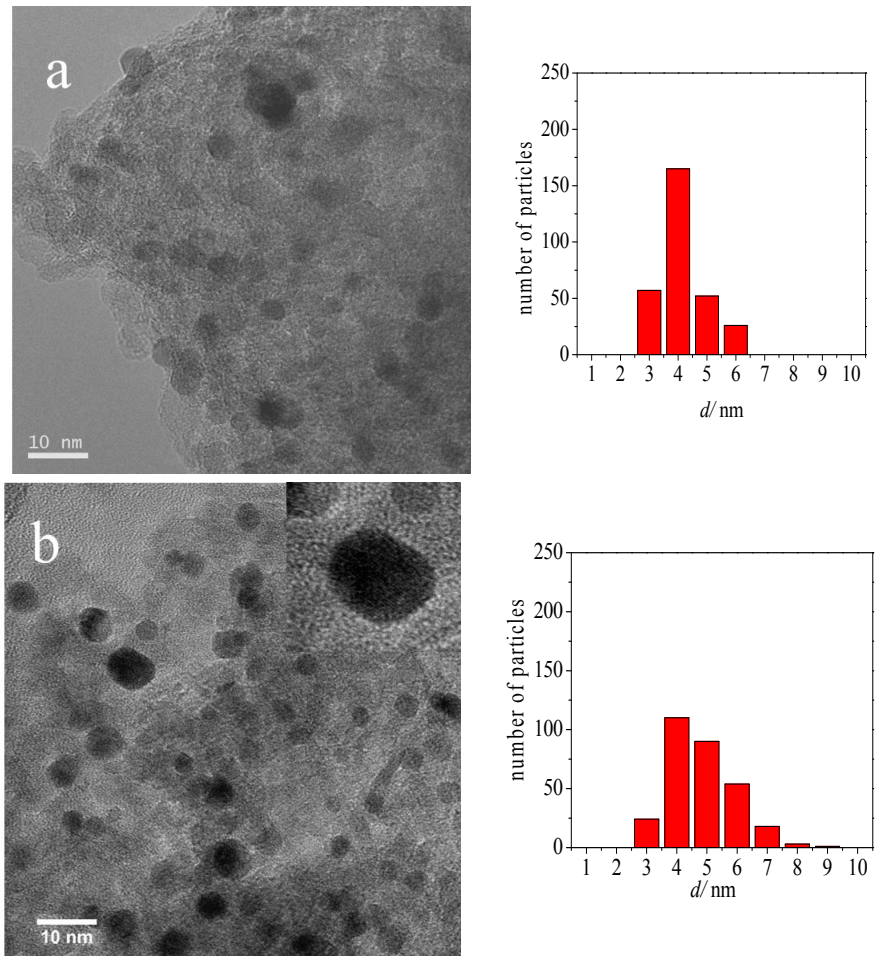

Figure 2. TEM images (left) and particle size distributions (right) of (**a**) Au-DDA/γ-Al_2O_3; and (**b**) Au-DDA/γ-Al_2O_3 (O_3 8 h). The inset in the TEM image (**b**) shows the crystallinity of an Au nanoparticle.

The TEM images of the catalysts after CO oxidation (Figure 3a,b) show that the high temperature CO oxidation caused some sintering. However, the particle size does not change drastically. The post-CO oxidation average particle size is 5.5 nm and 4.7 nm for Au-DDA/γ-Al_2O_3 and Au-DDA/γ-Al_2O_3 (O_3 8 h), respectively. The particle size analyses are summarised in Table 1. This indicates that removal of the stabilizing capping agent before submission to oxidising conditions decreases sintering of the Au nanoparticles. This stabilisation is due to the increased metal-support interaction after removal of the capping agent. When the capping agent is still present, it covers the whole Au nanoparticle, shielding its interaction with the support and leading to a decreased nanoparticle—support interaction, which in turn leads to increased mobility of the Au nanoparticles during the heating for the CO oxidation reaction; this in turn leads to an increased probability for sintering. Once the capping agent has been removed, the Au nanoparticle interacts directly with the support, leading to decreased mobility and thus decreased sintering. This was also observed by Elliott et al. [26], who showed an increase in Au nanoparticle size only when no more S signal from the residual capping agent was observed in XPS. The XPS data (discussed in more detail below) show that the as-prepared Au nanoparticles are metallic, whereas the ozone-treated Au nanoparticles are cationic. These cationic nanoparticles will have increased interaction with the oxidic support as compared to the metallic nanoparticles.

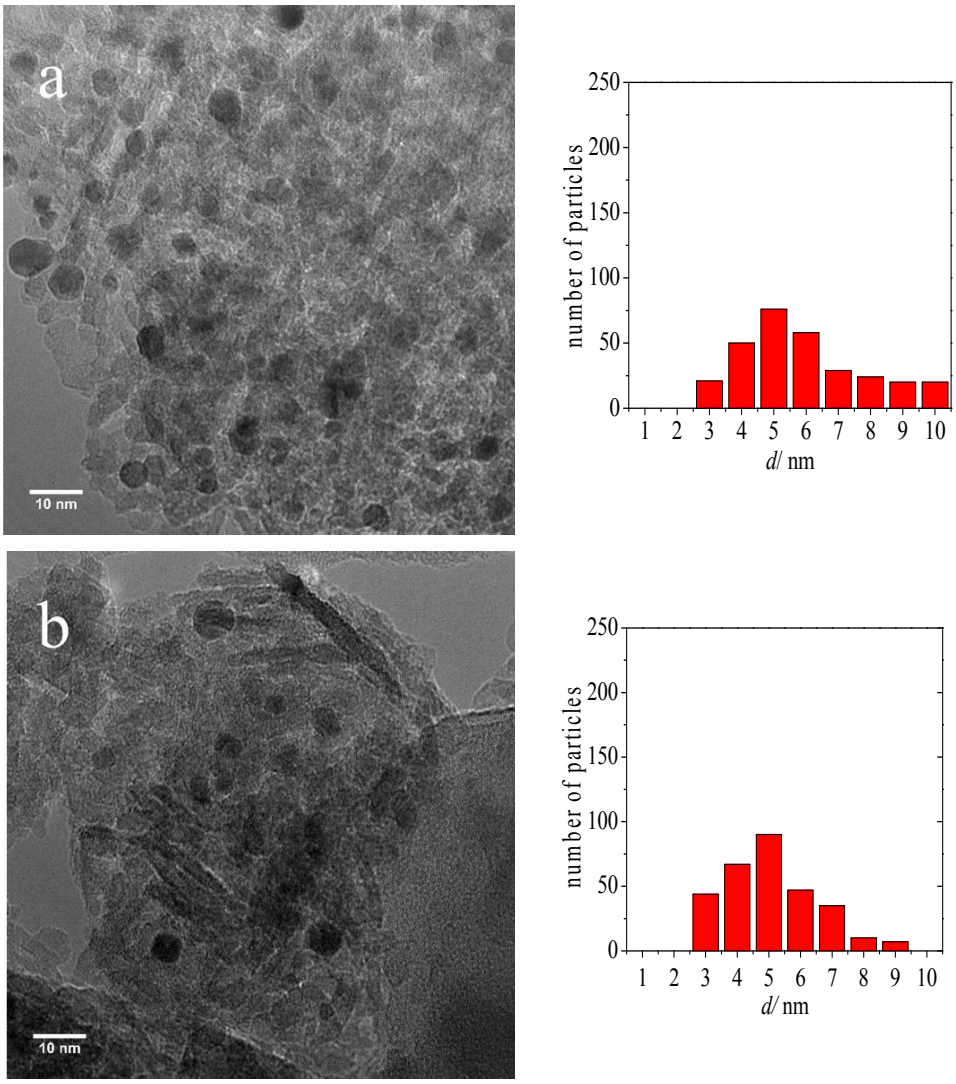

Figure 3. TEM images (right) and particle size distributions (left) of post-CO oxidation of (**a**) Au-DDA/γ-Al_2O_3; and (**b**) Au-DDA/γ-Al_2O_3 (O_3 8 h).

Table 1. Au particle size from TEM.

Sample	Average Au Particle Size (nm)	Standard Deviation (nm)
Au-DDA colloid	3.3	0.5
Au-DDA colloid (w)	3.8	0.5
Au-DDA/γ-Al_2O_3	4.0	0.8
Au-DDA/γ-Al_2O_3 (O_3 8 h)	4.3	1.0
Post-CO ox Au-DDA/γ-Al_2O_3	5.5	1.9
Post-CO ox Au-DDA/γ-Al_2O_3 (O_3 8 h)	4.7	1.3

Figure 4 shows infrared spectra of Au-DDA/γ-Al_2O_3 after different durations of ozone treatment. As shown in Figure 4, the peaks at 2858 cm^{-1} and 2930 cm^{-1} correspond to the vibration energy signals of $–CH_2–$ and $–CH_3$ groups from the DDA [39,40]. The intensity of these peaks disappeared after 7 h of treatment, showing that the DDA had been removed. To make sure that all of the DDA had been removed, 8 h of treatment was chosen as the experimental time to remove the DDA before performing catalytic reactions. The changes in the peaks below 1600 cm^{-1} are due to water vapour interactions on the surface of the γ-Al_2O_3 support. Combining the information from TEM and FTIR, we conclude that DDA was removed from the surface of the Au nanoparticles after 8 h of ozone treatment at 30 °C without drastically changing the diameter of the particles.

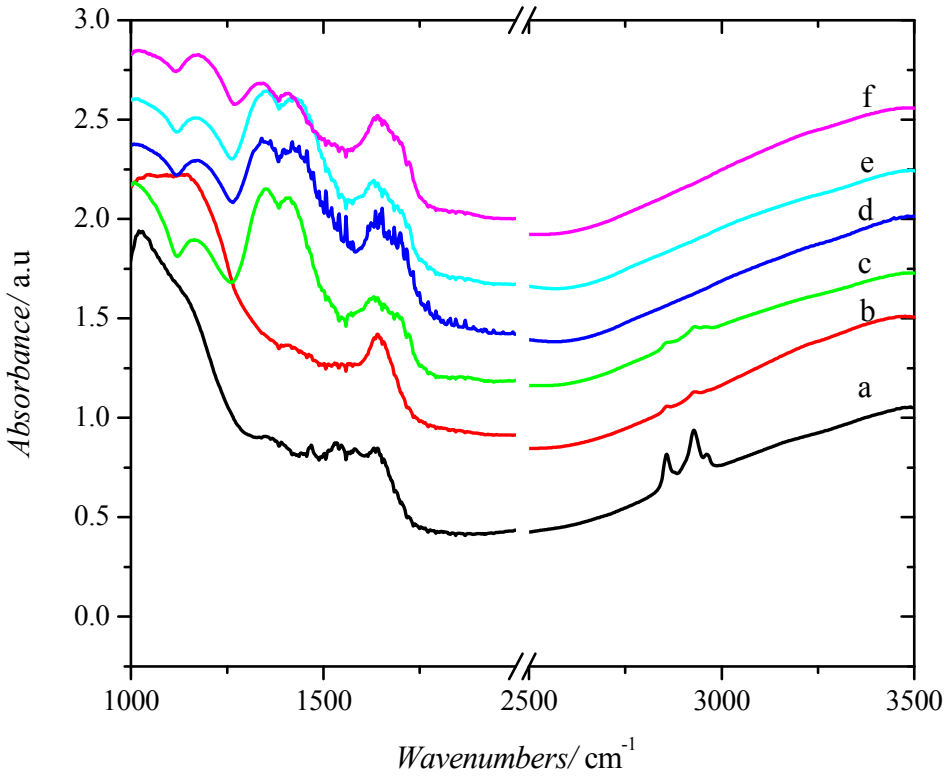

Figure 4. FTIR spectra of (**a**) DDA/γ-Al_2O_3; (**b**) Au-DDA/γ-Al_2O_3; (**c**) Au-DDA/γ-Al_2O_3 (O_3 6 h); (**d**) Au-DDA/γ-Al_2O_3 (O_3 7 h); (**e**) Au-DDA/γ-Al_2O_3 (O_3 8 h); and (**f**) Au-DDA/γ-Al_2O_3 (O_3 10 h).

XPS was used to study the oxidation state of the gold. Figure 5 shows the Au 4f photoelectron spectra of the Au-DDA/γ-Al_2O_3 and the ozone treated catalysts. For the ozone treated catalyst, the peaks shifted to higher binding energies. The full width at half maximum (FWHM) measurement of the deconvoluted peaks indicates that the Au in the as-prepared catalyst is metallic (Au^0), while after ozone treatment the Au is cationic ($Au^{\delta+}$). These results are in line with previous studies, which concluded that surfactant-encapsulated gold and platinum nanoparticles have a metallic surface, while

supported bare nanoparticles have a cationic surface [12,41–43]. Due to the small amount of capping agent present (only 1 wt % Au is present on the support material to start with), the XPS signal for N was too weak and noisy to be quantified.

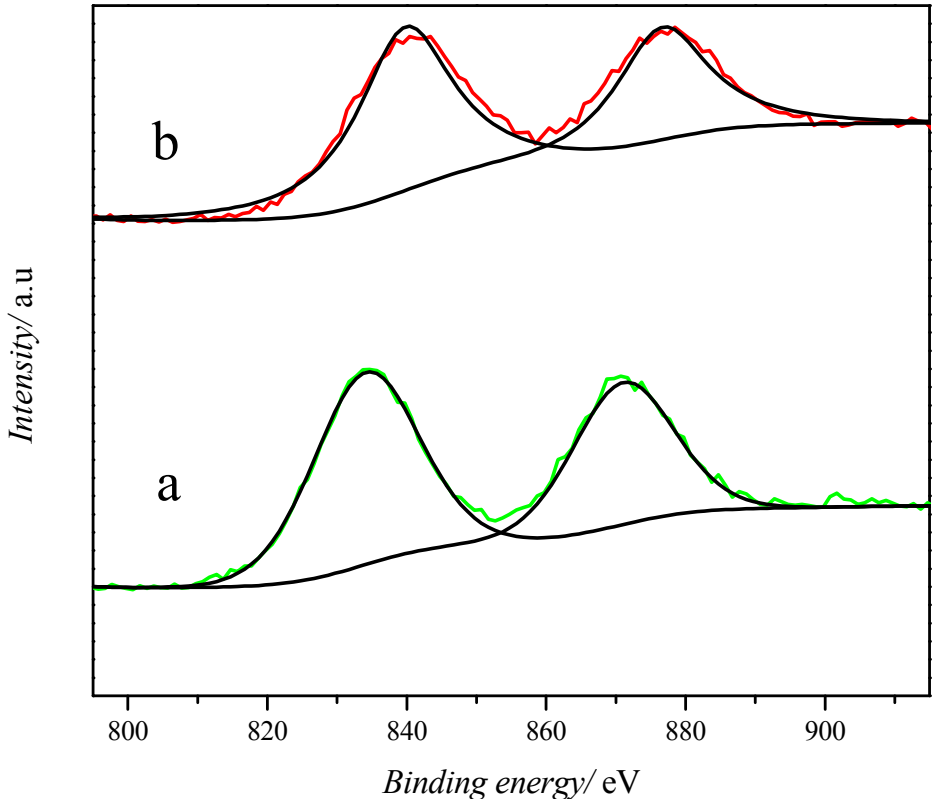

Figure 5. X-ray Photoelectron Spectroscopy (XPS) spectra of the Au 4f binding energy region for (**a**) Au-DDA/γ-Al_2O_3; and (**b**) Au-DDA/γ-Al_2O_3 (O_3 8 h).

2.2. Catalytic Performance

Figure 6 shows the CO conversion against temperature for several samples. The blank samples (γ-Al_2O_3 and DDA/γ-Al_2O_3) show very low conversion because the active phases for this reaction are the Au nanoparticles and the gold particle-support interaction [38,44]. The Au-DDA/γ-Al_2O_3 (O_3 8 h) ends up with a slightly higher catalytic activity than Au-DDA/γ-Al_2O_3, which matches with its slightly smaller Au particle size (4.7 versus 5.5 nm, see Figure 2). It is possible that the traces of chloride (from the Au precursor during catalyst preparation) that are present on the surface of the Au nanoparticles also lower the catalytic activity by stimulating the agglomeration of Au nanoparticles during the heat treatment and hinder the reduction of Au cations by poisoning [45–47]. The CO oxidation reaction has also been shown to be very sensitive to the Au particle size for a range of support materials [48]. The 1% AUROlite^{TM} catalyst, which has the smallest particle size of all catalysts studied here (reference catalyst, average particle size is 2.5 nm [49]), exhibits the highest CO oxidation activity. Figure 7 shows the CO oxidation performance of Au-DDA/γ-Al_2O_3 and Au-DDA/γ-Al_2O_3 (O_3 8 h) during heating and cooling. The CO conversion during cooling is slightly lower than during heating, which is attributed to the slight sintering observed by TEM. The small difference in activity is attributed to the fairly large (at least for this reaction) starting particle size. For CO oxidation, the largest effect of the particle size on the activity is observed for Au nanoparticles smaller than 4 nm [48].

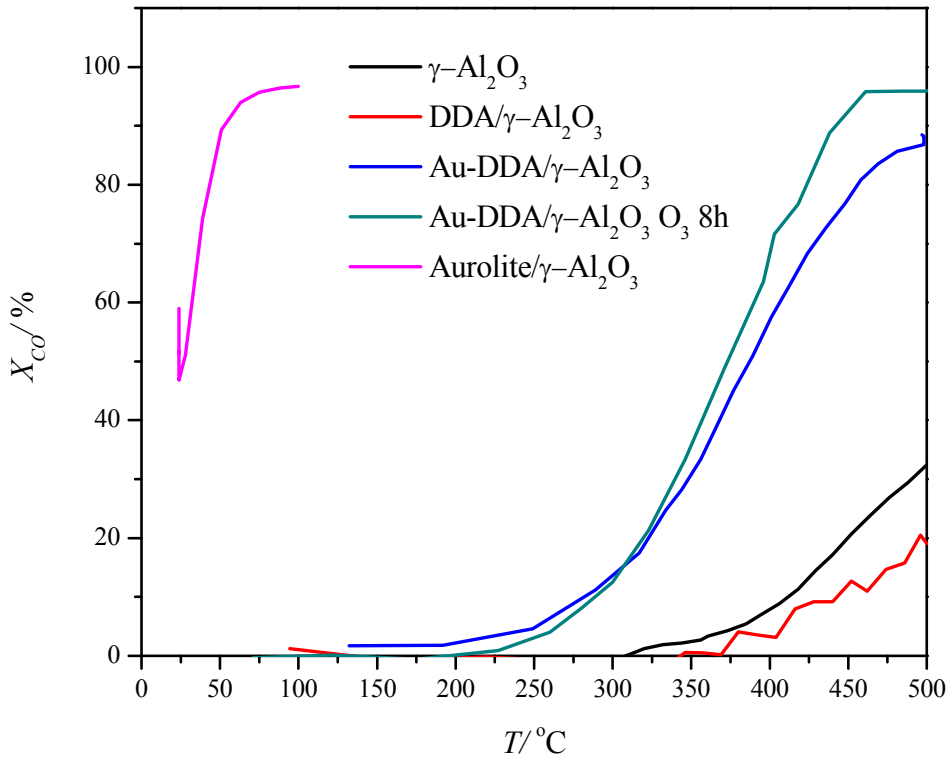

Figure 6. CO conversion versus temperature forγ-Al_2O_3; DDA/γ-Al_2O_3; Au-DDA/γ-Al_2O_3; Au-DDA/γ-Al_2O_3 (O_3 8 h); and AUROlite^{TM}.

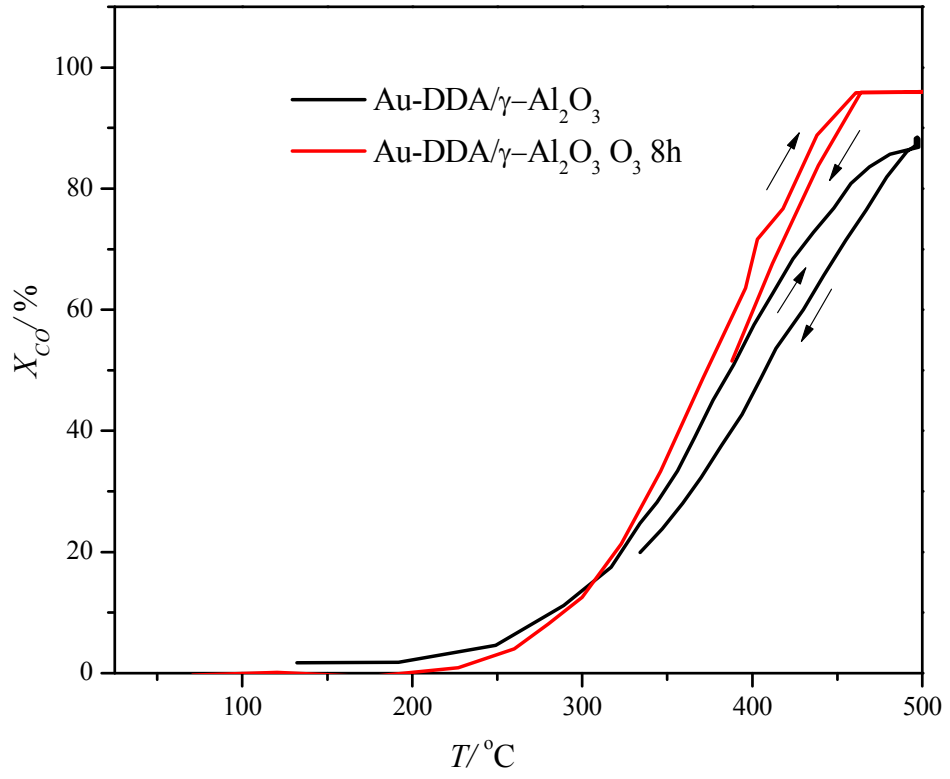

Figure 7. CO oxidation versus temperature during heating and cooling treatment Au-DDA γ-Al_2O_3; and Au-DDA/γ-Al_2O_3 (O_3 8 h).

The benzyl alcohol oxidation reaction is presented in Figure 8. The main product is benzaldehyde, while benzoic acid and benzyl benzoate are side products. The Au-DDA colloid is not active for this reaction, while supported Au-DDA shows some activity as reported in a previous study [12]. This confirms the metal-support interaction contributes to the catalytic activity. After capping agent removal, the interaction is stronger, therefore, the activity is slightly higher than for the as-prepared sample. Similar to the CO oxidation results, Au-DDA/γ-Al_2O_3 (O_3 8 h) is slightly more active than Au-DDA/γ-Al_2O_3: the turnover frequency (TOF) changes from 894 h^{-1} to 1106 h^{-1} upon removal of the capping agent. The benzyl alcohol conversions at 240 min are in the range of 65%−70% (Figure 9). For comparison, AUROlite^{TM} benzyl alcohol conversion at 240 min is 78% and its *TOF* is 682 h^{-1} [49].

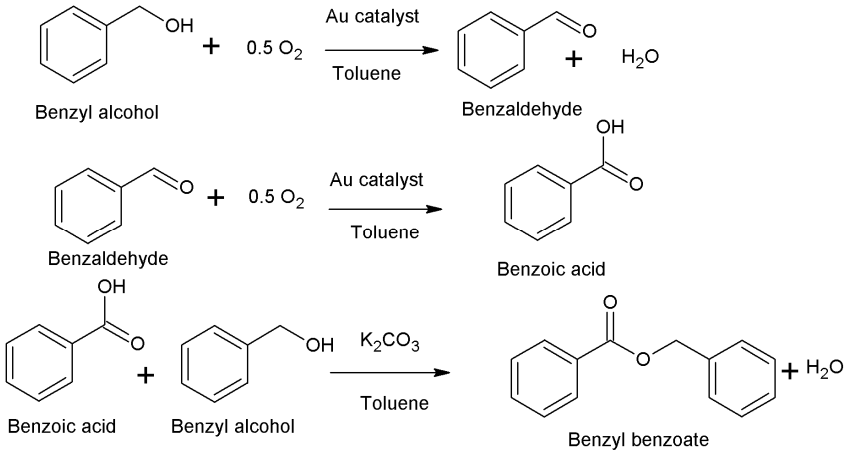

Figure 8. Benzyl alcohol oxidation pathways.

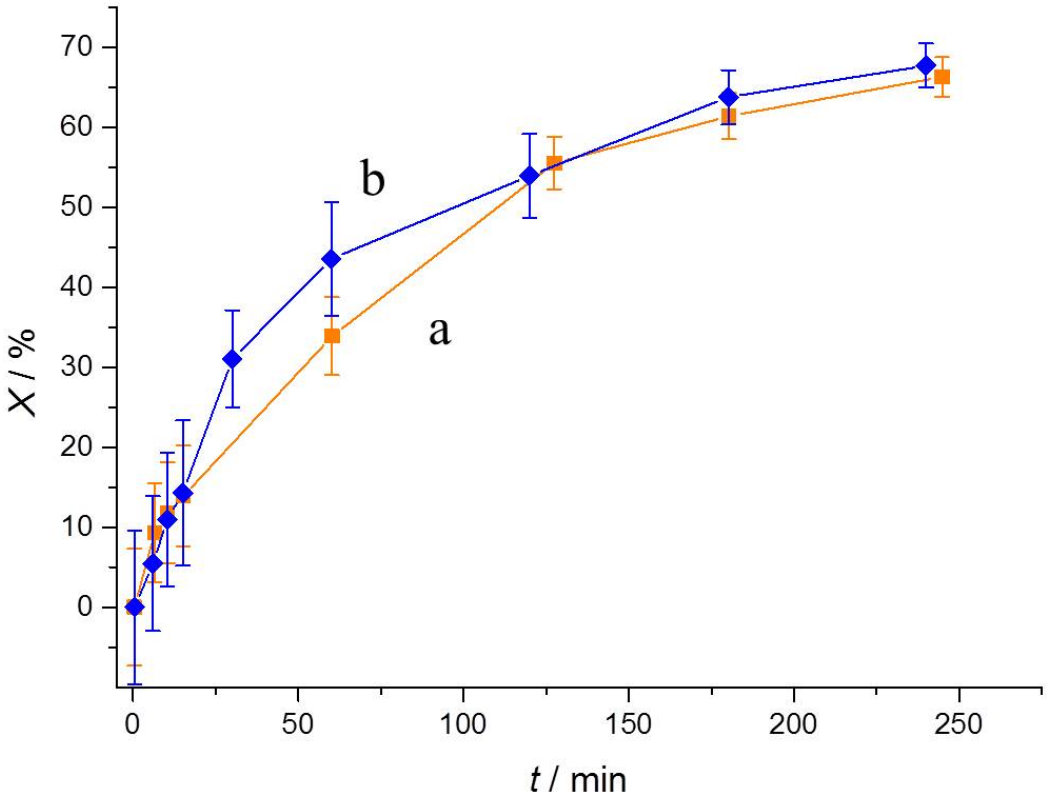

Figure 9. Benzyl alcohol conversion as a function of reaction time for (**a**) Au-DDA/γ-Al_2O_3 and (**b**) Au-DDA/γ-Al_2O_3 (O_3 8 h).

3. Materials and Methods

3.1. Catalyst Preparation

The gold catalysts were prepared following the methodology described by Chen [7] and Quintanilla [12]. The subsequent reactions taking place in the mixture are shown in Figure 10.

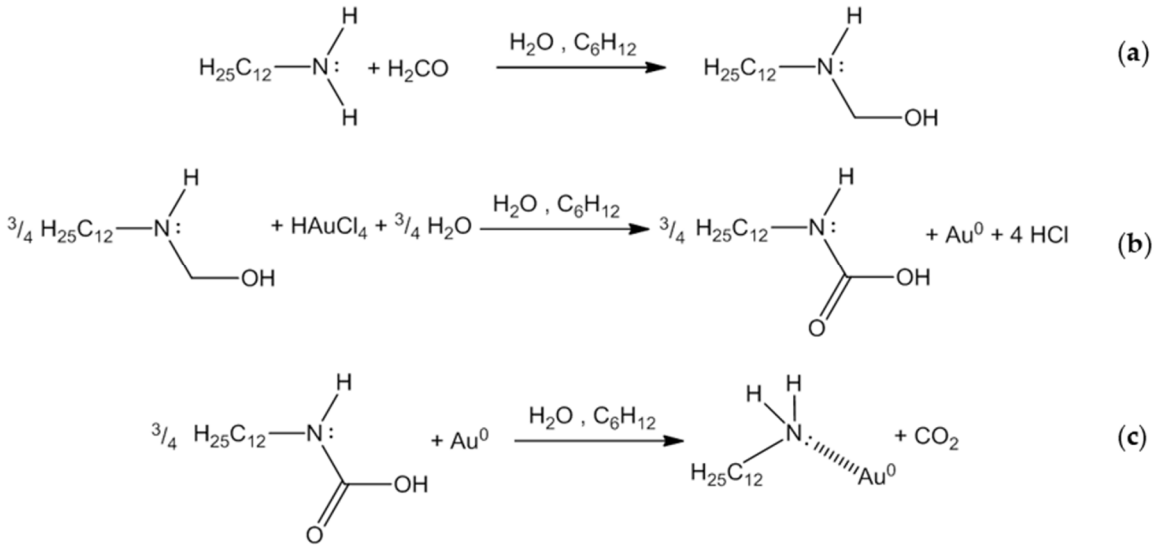

Figure 10. Au-DDA formation mechanism. (**a**) formation of the reductive intermediate dodecylaminomethanol from DDA and formaldehyde, (**b**) Reduction of gold precursor $HAuCl_4$ to metallic gold and oxidation of dodecylaminomethanol into dodecylcarbamic acid and (**c**) decomposition of dodecylcarbamic acid into DDA and interaction of the latter with metallic gold.

For step (a) of Figure 10, 0.75 g of DDA (99.5%, Sigma-Aldrich, St. Louis, MO, USA) was dissolved in 25 mL of cyclohexane (anhydrous, 99.5%, Sigma Aldrich), then 6 mL of formaldehyde solution (37 wt % in water, 10%–15% methanol as stabilizer, Sigma-Aldrich) was added to the mixture. This biphasic mixture was vigorously stirred at room temperature for 30 min. The two phases were allowed to phase separate in a decantation funnel. The top phase (transparent) was the cyclohexane phase and contained the desired dodecylaminomethanol (DDAM). The bottom phase (white) was the water phase, and contained the excess formaldehyde. After recovering the cyclohexane phase, 10 mL of 4 g/L $HAuCl_4$ (Sigma-Aldrich) in Milli-Q water was added under vigorous stirring at room temperature to induce steps (b) and (c) of Figure 10. Soon after addition, the suspension turned yellow. The DDAM was oxidized to the corresponding carbamic acid by Au^{3+}, which thereby reduced to Au^0 (step (b) of Figure 10). The carbamic acid was not stable and decomposed into the starting DDA and CO_2 (also in step (b) of Figure 10). DDA was then released and adsorbed on the Au^0 nanoparticle surface (step (c) of Figure 10). After stirring for at least 1 hour, the colour changed to ruby red, indicating the formation of small gold particles.

During stirring, two phases of suspensions were formed. The upper phase (ruby red) was the cyclohexane phase, which contained the Au-DDA, and the bottom phase was the water phase. The mixture was allowed to phase separate overnight in a decantation funnel. The result was a ruby red suspension of Au-DDA colloid in cyclohexane. This original colloid is referred to as "Au-DDA colloid". Subsequently, the Au-DDA colloid was washed using acetone. The acetone (about 3× the colloid volume) was added to the colloid suspension and after mixing the mixture was centrifuged for 5 min at 10,000 rpm to precipitate the nanoparticles. After disposal of the supernatant, the nanoparticles were re-dispersed in 25 mL of cyclohexane. This washed colloid is referred to as "Au-DDA colloid (w)".

The Au-DDA colloid (w) was immobilized on γ-Al_2O_3 by adding 1.5 g of previously calcined (500 °C, 6 h) γ-Al_2O_3 (<71 micron, Akzo Chemicals, Amsterdam, The Netherlands) to the cyclohexane mixture and stirring vigorously overnight. The suspension was filtered, resulting in a pink catalyst powder, which is denoted "Au-DDA/γ-Al_2O_3". The liquid phase was pale pink, so not all Au was absorbed on the powder. The powder was washed with 100 mL of cyclohexane and 100 mL of acetone, then left to dry in an evacuated desiccator at room temperature overnight.

Blank catalysts (γ-Al_2O_3 and DDA/γ-Al_2O_3) were also prepared, and commercial catalyst extrudates (AUROlite^{TM}, 1 wt % Au/γ-Al_2O_3, Strem Chemicals, Newburyport, MA, USA) were crushed and sieved to <71 micron to be used for comparison catalytic experiments.

3.2. Capping Agent Removal

The ozone treatment for capping agent removal was performed by loading the 1% Au-DDA/γ-Al_2O_3 catalyst into a custom-made U-tube glass reactor, which was installed in the oven (Binder FP53, Tuttlingen, Germany) of the ozone setup (Figure 11). Oxygen from a gas cylinder was passed through a Corona discharge ozone generator (A2Z Ozone Systems, SOZ-16GLAB, Louisville, KY, USA). The check valves (CV1 and CV2) prevent back-flow of the ozone to the mass flow controllers (MFC1 and MFC2, Bronkhorst High-Tech B.V., Ruurlo, The Netherlands). The ozone concentration at the outlet was monitored using an ozone detector (Lenntech, BMT 964, Delft, The Netherlands), after which it was sent through a manganese dioxide/copper oxide catalytic ozone destructor. Capping agent removal was conducted at 30 °C with an ozone concentration of 7 g/Nm^3 (0.35%). The reaction time was varied from 6 to 10 h. These catalysts are denoted as "Au-DDA/γ-Al_2O_3 (O_3, x h)", with x indicating the number of hours of ozone treatment.

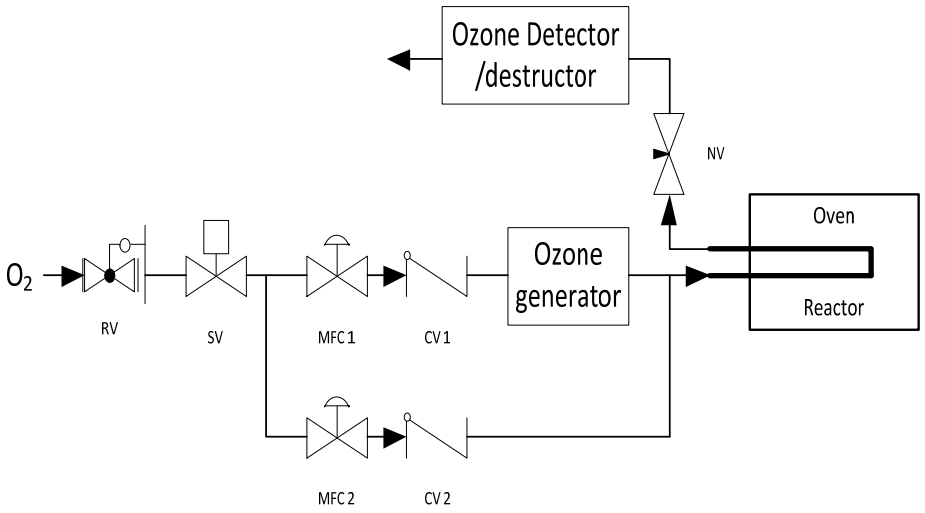

Figure 11. Scheme of the ozone setup.

3.3. Catalyst Characterization

The morphological characterization of the gold catalysts was performed using an FEI TECNAI F20 transmission electron microscope (Hillsboro, OR, USA) equipped with a Field Emission Gun (FEG) and a Gatan ultrascan camera, operated at 200 kV. The samples were prepared by depositing a drop of colloid or finely crushed catalyst suspension in ethanol onto a Quantifoil® carbon film (Jena, Germany) supported on a copper TEM microgrid and leaving it to dry at room temperature. The particle size distributions and average particle sizes were determined from the TEM images by measuring the size of 300 individual particles for each sample.

The infrared spectra of the catalysts were recorded using a Thermo Scientific Nicolet Fourier Transformed Infrared (FTIR) spectrophotometer (Waltham, MA, USA). Prior to the FTIR

characterization, the background spectrum of pure KBr powder was recorded under He flow at room temperature. Then about 0.050 g of catalyst was evenly spread on top of the KBr powder. The KBr background spectrum was automatically subtracted from the spectrum obtained from the measurement, resulting in the sample spectrum only.

The catalyst oxidation states were studied using a Thermo Scientific K-Alpha X-ray photoelectron spectrometer (XPS, Waltham, MA, USA). The XPS spectra were recorded at ambient temperature at a chamber pressure of about 10^{-7} mbar, using a line scan of four points with each point having a spot size of 400 μm. The binding energy of the XP spectra was calibrated using the C 1 s peak (binding energy = 285.1 eV). The spectra were analysed and processed using Thermo Avantage v5.903 software (Thermo Scientific, Waltham, MA, USA). The peaks were fit using a Lorentzian-Gaussian product function. A Shirley-type background was then subtracted from the spectra and the Au 4f spectra were deconvoluted.

3.4. Catalytic Reactions

For the CO oxidation, approximately 25 mg of catalyst mixed with ~100 mg SiC was placed into a tubular glass reactor (inner diameter ~0.4 mm) and sandwiched between two layers of ~50 mg SiC and quartz wool. The experiments were performed at 2 bar total pressure with a gas flow of 0.5% O_2, 1% CO, and 98.5% He at 35 mL/min. The reaction temperature was increased by 5 °C/min from room temperature to 300 °C, then by 1 °C/min from 300 °C to 500 °C. After 1 h at 500 °C, the reactor was cooled down to 330 °C by 1 °C/min. The outlet stream was analysed every 12 min using a Chrompack CP 9001 gas chromatograph equipped with a TCD (Agilent Technologies, Santa Clara, CA, USA). Helium was used as a carrier gas through a dual column system consisting of a Parabond Q column (Chrompack, 25 m in length, 0.53 mm in diameter and 10 μm of coating thickness) and a Molsieve 5A column (Chrompack, 10 m in length, 0.53 mm in diameter and 50 μm of coating thickness). The CO oxidation reaction using a reference catalyst (1% Aurolite from Strem Chemicals) and blank experiments (using γ-Al_2O_3 and DDA/γ-Al_2O_3) was also performed for comparison.

Another reaction to evaluate catalytic performance was benzyl alcohol oxidation. In a round-bottom flask (60 mm inner diameter, equipped with baffles and stirrer shaft), approximately 0.6 g of catalyst was mixed with 3.04 g of K_2CO_3 (>99.0%, Sigma-Aldrich). Eighty millilitres of toluene (anhydrous, 99.8%, Sigma Aldrich) was added to disperse the mixture. The flask was stirred at 1200 rpm and heated to 80 °C, and 200 mL/min of air was bubbled through the mixture. When the temperature was stable, 22 mmol (2.4 g) of benzyl alcohol was added (t = 0 min). Small samples of 300 μL were taken at recorded times and filtered from catalyst and K_2CO_3 powders with a syringe Teflon filter (diameter: 13 mm; pore size: 0.2 μm; PTFE membrane; VWR International, Radnor, PA, USA) and introduced in a GC sample vial together with 20 μL of tetradecane, the latter being used as an internal standard. They were analysed using a Varian CP-3380 gas chromatograph equipped with a FID (Agilent Technologies, Santa Clara, CA, USA). Helium was used as carrier gas through a CP-SIL 8 CB column (Chrompack) of 50 m in length, 0.25 mm in diameter, and with 0.25 μm coating thickness. No blank experiments were performed because previous work showed that no conversion of benzyl alcohol occurs over pure γ-Al_2O_3. The turnover frequency (*TOF*) was calculated as follows:

$$TOF = \frac{\Delta n_{BnOH}}{\Delta t} \times \frac{M_{Au}}{w_{cat} \times x_{Au}}$$

where $\frac{\Delta n_{BnOH}}{\Delta t}$ is the benzyl alcohol reaction rate (mol/h), M_{Au} is the molar mass of gold (g/mol), w_{cat} is the amount of catalyst in the reactor (g), and x_{Au} is the gold loading of the catalyst (wt %).

4. Conclusions

Ozone treatment at mild temperature was shown to remove the capping agent from the surface of supported gold nanoparticles. The average particle size, shape, and crystallinity of the gold

nanoparticles hardly changed after capping agent removal. Due to the mild temperature of the ozone treatment, sintering was minimised and stable catalytic particles were obtained. The ozone treated catalysts did not sinter significantly even during the high temperature CO oxidation reaction, whereas the as-prepared capping agent containing catalyst was affected by sintering and, thus, showed lower activity. The activity for benzyl alcohol oxidation with molecular oxygen of the ozone-treated Au-DDA γ-Al_2O_3 was slightly increased compared to that of the as-prepared catalyst, probably due to the increased concentration of Au cationic species on the surface of the catalyst after the ozone treatment. Repeated catalytic tests are required to analyse the possibility of long-term deactivation processes due to sintering on both catalysts.

Acknowledgments: The Dutch National Research School Combination Catalysis Controlled by Chemical Design (NRSC-Catalysis) and the NIMIC SmartMix consortium are gratefully acknowledged for financial support. B. van der Linden is acknowledged for practical support.

Author Contributions: P.J.K. and F.K. conceived and designed the experiments; I.P. and E.S. performed the experiments and analysed the data; all authors contributed to writing the paper.

Conflicts of Interest: The authors declare no conflict of interest.

References

1. Hutchings, G.J.; Haruta, M. A golden age of catalysis: A perspective. *Appl. Catal. A* **2005**, *291*, 2–5. [CrossRef]
2. Geoffrey, C.B.; Catherine, L.; David, T.T. *Catalysis by Gold*; Imperial College Press: London, UK, 2006.
3. Otieno, B.A.; Krause, C.E.; Latus, A.; Chikkaveeraiah, B.V.; Faria, R.C.; Rusling, J.F. On-line protein capture on magnetic beads for ultrasensitive microfluidic immunoassays of cancer biomarkers. *Biosens. Bioelectron.* **2014**, *53*, 268–274. [CrossRef] [PubMed]
4. Nagelli, E.; Naik, R.; Xue, Y.; Gao, Y.; Zhang, M.; Dai, L. Sensor arrays from multicomponent micropatterned nanoparticles and graphene. *Nanotechnology* **2013**, *24*, 444010. [CrossRef] [PubMed]
5. Lee, I.; Morales, R.; Albiter, M.A.; Zaera, F. Synthesis of heterogeneous catalysts with well shaped platinum particles to control reaction selectivity. *Proc. Natl. Acad. Sci. USA* **2008**, *105*, 15241–15246. [CrossRef] [PubMed]
6. Polavarapu, L.; Xu, Q.H. A simple method for large scale synthesis of highly monodisperse gold nanoparticles at room temperature and their electron relaxation properties. *Nanotechnology* **2009**, *20*, 185606. [CrossRef] [PubMed]
7. Chen, Y.; Wang, X. Novel phase-transfer preparation of monodisperse silver and gold nanoparticles at room temperature. *Mater. Lett.* **2008**, *62*, 2215–2218. [CrossRef]
8. Sun, Y.; Mayers, B.; Herricks, T.; Xia, Y. Polyol synthesis of uniform silver nanowires: A plausible growth mechanism and the supporting evidence. *Nano Lett.* **2003**, *3*, 955–960. [CrossRef]
9. Sun, Y.; Xia, Y. Shape-controlled synthesis of gold and silver nanoparticles. *Science* **2002**, *298*, 2176–2179. [CrossRef] [PubMed]
10. Bratlie, K.M.; Lee, H.; Komvopoulos, K.; Yang, P.; Somorjai, G.A. Platinum nanoparticle shape effects on benzene hydrogenation selectivity. *Nano Lett.* **2007**, *7*, 3097–3101. [CrossRef] [PubMed]
11. Tao, A.R.; Habas, S.; Yang, P. Shape control of colloidal metal nanocrystals. *Small* **2008**, *4*, 310–325. [CrossRef]
12. Quintanilla, A.; Butselaar-Orthlieb, V.C.L.; Kwakernaak, C.; Sloof, W.G.; Kreutzer, M.T.; Kapteijn, F. Weakly bound capping agents on gold nanoparticles in catalysis: Surface poison? *J. Catal.* **2010**, *271*, 104–114. [CrossRef]
13. Lange, C.; De Caro, D.; Gamez, A.; Storck, S.; Bradley, J.S.; Maier, W.F. Polymer-induced selectivity enhancement in the hydrogenation of 2-hexyne catalyzed by poly(vinylpyrrolidone)-stabilized platinum colloids in an amorphous mixed metal oxide support. *Langmuir* **1999**, *15*, 5333–5338. [CrossRef]
14. Imura, Y.; Furukawa, S.; Ozawa, K.; Morita-Imura, C.; Kawaib, T.; Komatsu, T. Surface clean gold nanoflower obtained by complete removal of capping agents: An active catalyst for alcohol oxidation. *RCS Adv.* **2016**, *6*, 17222–17227. [CrossRef]
15. Zhong, Z.; Teo, J.; Lin, M.; Ho, J. Synthesis of Porous α-Fe_2O_3 Nanorods as Catalyst Support and a Novel Method to Deposit Small Gold Colloids on them. *Top. Catal.* **2008**, *49*, 216–226. [CrossRef]

16. Chen, Y.; Hassel, A.W.; Erbe, A. Enhancement of the Electrocatalytic Activity of Gold Nanoparticles towards Methanol Oxidation. *Electrocatal* **2011**, *2*, 106–113. [CrossRef]
17. Naresh, N.; Wasim, F.G.S.; Ladewig, B.P.; Neergat, M. Removal of surfactant and capping agent from Pd nanocubes (Pd-NCs) using tert-butylamine: Its effect on electrochemical characteristics. *J. Mater. Chem. A* **2013**, *1*, 8553–8559. [CrossRef]
18. Mazumder, V.; Sun, S. Oleylamine-mediated synthesis of Pd nanoparticles for catalytic formic acid oxidation. *JACS* **2009**, *131*, 4588–4589. [CrossRef] [PubMed]
19. Nalajala, N.; Gooty Saleha, W.F.; Ladewig, B.P.; Neergat, M. Sodium borohydride treatment: A simple and effective process for the removal of stabilizer and capping agents from shape-controlled palladium nanoparticles. *Chem. Commun.* **2014**, *50*, 9365–9368. [CrossRef] [PubMed]
20. Niu, Z.; Li, Y.P. Removal and utilization of capping agents in nanocatalysis. *Chem. Mater.* **2014**, *26*, 72–83. [CrossRef]
21. Kuhn, J.; Gascon, J.; Gross, J.; Kapteijn, F. Detemplation of DDR type zeolites by ozonication. *Micropor. Mesopor Mat.* **2009**, *120*, 12–18. [CrossRef]
22. Heng, S.; Lau, P.P.S.; Yeung, K.L.; Djafer, M.; Schrotter, J.C. Low-temperature ozone treatment for organic template removal from zeolite membrane. *J. Membr. Sci.* **2004**, *243*, 69–78. [CrossRef]
23. Benson, S.W.; Axworthy, A.E. Reconsideration of the rate constants from the thermal decomposition of ozone. *J. Chem. Phys.* **1965**, *42*, 2614–2615. [CrossRef]
24. Benson, S.W.; Axworthy, A.E., Jr. Mechanism of the gas phase, thermal decomposition of ozone. *J. Chem. Phys.* **1957**, *26*, 1727–1733. [CrossRef]
25. Menard, L.D.; Xu, F.; Nuzzo, R.G.; Yang, J.C. Preparation of TiO_2-supported Au nanoparticle catalysts from a Au_{13} cluster precursor: Ligand removal using ozone exposure versus a rapid thermal treatment. *J. Catal.* **2006**, *243*, 64–73. [CrossRef]
26. Elliott, E.W., III; Glover, R.D.; Hutchison, J.E. Removal of Thiol Ligands from surface-confined nanoparticles without particle growth or desorption. *ACS Nano* **2015**, *9*, 3050–3059. [CrossRef] [PubMed]
27. Nijhuis, T.A.; Sacaliuc, E.; Beale, A.M.; van der Eerden, A.M.J.; Schouten, J.C.; Weckhuysen, B.M. Spectroscopic evidence for the adsorption of propene on gold nanoparticles during the hydro-epoxidation of propene. *J. Catal.* **2008**, *258*, 256–264. [CrossRef]
28. Delannoy, L.; Fajerwerg, K.; Lakshmanan, P.; Potvin, C.; Méthivier, C.; Louis, C. Supported gold catalysts for the decomposition of VOC: Total oxidation of propene in low concentration as model reaction. *Appl. Catal. B* **2010**, *94*, 117–124. [CrossRef]
29. Valden, M.; Lai, X.; Goodman, D.W. Onset of catalytic activity of gold clusters on titania with the appearance of nonmetallic properties. *Science* **1998**, *281*, 1647–1650. [CrossRef] [PubMed]
30. Go, M.J.; Lee, B.K.; Kumar, P.A.; Lee, W.K.; Joo, O.S.; Ha, H.P.; Lim, H.B.; Hur, N.H. Immobilization of nanocatalysts on cordierite honeycomb monoliths for low temperature NO_x reduction. *Appl. Catal. A* **2009**, *370*, 102–107. [CrossRef]
31. Miquel, P.; Granger, P.; Jagtap, N.; Umbarkar, S.; Dongare, M.; Dujardin, C. NO reduction under diesel exhaust conditions over Au/Al_2O_3 prepared by deposition-precipitation method. *J. Mol. Catal. A Chem.* **2010**, *322*, 90–97. [CrossRef]
32. Sárkány, A. Acetylene hydrogenation on SiO_2 supported gold nanoparticles. *React. Kinet. Catal. Lett.* **2009**, *96*, 43–54. [CrossRef]
33. Gluhoi, A.C.; Bakker, J.W.; Nieuwenhuys, B.E. Gold, still a surprising catalyst: Selective hydrogenation of acetylene to ethylene over Au nanoparticles. *Catal. Today* **2010**, *154*, 13–20. [CrossRef]
34. Mohamed, M.; Khairou, K.S. Morphological characteristics of gold nanowires and nanoparticles: Structure elucidation and reactivity toward water-gas shift reaction. *Energy Fuel* **2009**, *23*, 4413–4419. [CrossRef]
35. Rodriguez, J.A. Gold-based catalysts for the water-gas shift reaction: Active sites and reaction mechanism. *Catal. Today* **2011**, *160*, 3–10. [CrossRef]
36. Lu, P.; Teranishi, T.; Asakura, K.; Miyake, M.; Toshima, N. Polymer-protected Ni/Pd bimetallic nano-clusters: Preparation, characterization and catalysis for hydrogenation of nitrobenzene. *J. Phys. Chem. B* **1999**, *103*, 9673–9682. [CrossRef]
37. Sun, Y.; Xia, Y. Large-scale synthesis of uniform silver nanowires through a soft, self-seeding, polyol process. *Adv. Mater.* **2002**, *14*, 833–837. [CrossRef]

38. Comotti, M.; Li, W.C.; Spliethoff, B.; Schüth, F. Support effect in high activity gold catalysts for CO oxidation. *JACS* **2006**, *128*, 917–924. [CrossRef] [PubMed]
39. Mo, L.; Liu, D.; Li, W.; Li, L.; Wang, L.; Zhou, X. Effects of dodecylamine and dodecanethiol on the conductive properties of nano-Ag films. *Appl. Surf. Sci.* **2011**, *257*, 5746–5753. [CrossRef]
40. Dablemont, C.; Lang, P.; Mangeney, C.; Piquemal, J.Y.; Petkov, V.; Herbst, F.; Viau, G. FTIR and XPS study of Pt nanoparticle functionalization and interaction with alumina. *Langmuir* **2008**, *24*, 5832–5841. [CrossRef] [PubMed]
41. Leff, D.V.; Brandt, L.; Heath, J.R. Synthesis and characterization of hydrophobic, organically-soluble gold nanocrystals functionalized with primary amines. *Langmuir* **1996**, *12*, 4723–4730. [CrossRef]
42. Borodko, Y.; Habas, S.E.; Koebel, M.; Yang, P.; Frei, H.; Somorjai, G.A. Probing the interaction of poly(vinylpyrrolidone) with platinum nanocrystals by UV-Raman and FTIR. *J. Phys. Chem. B* **2006**, *110*, 23052–23059. [CrossRef] [PubMed]
43. Calla, J.T.; Davis, R.J. X-ray absorption spectroscopy and CO oxidation activity of Au/Al_2O_3 treated with NaCN. *Catal. Lett.* **2005**, *99*, 21–26. [CrossRef]
44. Liu, X.; Liu, M.H.; Luo, Y.C.; Mou, C.Y.; Lin, S.D.; Cheng, H.; Chen, J.M.; Lee, J.F.; Lin, T.S. Strong metal-support interactions between gold nanoparticles and ZnO nanorods in CO oxidation. *JACS* **2012**, *134*, 10251–10258. [CrossRef] [PubMed]
45. Oxford, S.M.; Henao, J.D.; Yang, J.H.; Kung, M.C.; Kung, H.H. Understanding the effect of halide poisoning in CO oxidation over Au/TiO_2. *Appl. Catal. A* **2008**, *339*, 180–186. [CrossRef]
46. Oh, H.S.; Yang, J.H.; Costello, C.K.; Wang, Y.M.; Bare, S.R.; Kung, H.H.; Kung, M.C. Selective catalytic oxidation of CO: Effect of chloride on supported Au catalysts. *J. Catal.* **2002**, *210*, 375–386. [CrossRef]
47. Lin, C.H.; Lin, S.D.; Lee, J.F. Chlorine residue in the Au/γ-Al_2O_3 prepared by $AuCl_3$ impregnation—An EXAFS analysis. *Catal. Lett.* **2003**, *89*, 235–242. [CrossRef]
48. Lopez, N.; Janssens, T.V.W.; Clausen, B.S.; Xu, Y.; Macrikakis, M.; Bligaard, T.; Nørskov, J.K. On the origin of the catalytic activity of gold nanoparticles for low-temperature CO oxidation. *J. Catal.* **2004**, *223*, 232–235. [CrossRef]
49. Skupien, E.; Berger, R.; Santos, V.; Gascon, J.; Makkee, M.; Kreutzer, M.T.; Kooyman, P.J.; Moulijn, J.A.; Kapteijn, F. Inhibition of a gold-based catalyst in benzyl alcohol oxidation: Understanding and remediation. *Catalysts* **2014**, *4*, 89–115. [CrossRef]